Intermetallics 60 (2015) 1–8

Contents lists available at ScienceDirect

Intermetallics

journal homepage: www.elsevier.com/locate/intermet

Effects of Nb additions on the microstructure and mechanical property of CoCrFeNi high-entropy alloys

W.H. Liu [a, b], J.Y. He [b], H.L. Huang [b], H. Wang [b, *], Z.P. Lu [b], C.T. Liu [a, *]

[a] Center for Advanced Structural Materials, Department of Mechanical and Biomedical Engineering, City University of Hong Kong, Hong Kong, PR China
[b] State Key Laboratory for Advance Metals and Materials, University of Science and Technology Beijing, Beijing 10083, PR China

ARTICLE INFO

Article history:
Received 19 November 2014
Received in revised form
8 January 2015
Accepted 9 January 2015
Available online 24 January 2015

Keywords:
A.High–entropy alloys
B.Phase stability
D.Microstructure
E.Mechanical properties

ABSTRACT

A series of five-component $CoCrFeNiNb_x$ high entropy alloys (HEAs) were synthesized to investigate alloying effects of the large atom Nb on the structure and tensile properties. Microstructures of these alloys were examined using scanning electron microscopy and the phase evolution was characterized and compared using the ΔH_{mix}–δ and ΔX criteria. It was found that the microstructure changes from the initial single face-centered cubic (FCC) to duplex FCC plus hexagonal close-packed (HCP) structure with additions of Nb. The current alloy system exhibits a hypoeutectic structure and the volume fraction of the Nb-enriched Laves phase with the HCP structure increases with increasing the Nb content, which is mainly responsible for the increment in the yield and fracture strength. Particularly, the $Nb_{0.155}$ alloy containing a 9.3% Nb-enriched Laves phase exhibits the most promising mechanical properties with the yield strength and plastic strain as high as 321 MPa and 21.3%, respectively. The ΔH_{mix}–δ criteria well describe the phase selection for the thermally treated alloys, while the physical parameter ΔX fails to predict the appearance of the Nb-enriched Laves phase in this alloy system.

1. Introduction

In recent years, one kind of new alloy, i.e., high entropy alloys (HEAs), has attracted extensive research attention because of their unusual properties [1]. These HEAs generally exhibit remarkable mechanical properties, including high strength, good wear and corrosion resistance, and high-temperature softening resistance [1–5]. Against the expectation to form various intermetallic compounds from general physical metallurgy principles, these compositionally complex alloys actually form simple solid solutions with FCC and/or body-centered cubic (BCC) structures [1,6–8], which are often believed to be resulted from their high mixing entropy. However, many experimental evidences revealed that ordered solid solutions and/or intermetallic phases may also exist in some HEAs [2,6,9,10], especially in the alloys that contain atomic pairs with large enthalpy of mixing and atomic size differences. These observations indicate that the high entropy of mixing of the alloying elements is simply not sufficient to prevent the formation of intermetallic phases in favor of solid solution phases in HEAs [11,12].

Hume-Rothery generalized several rules on substitutional solid solutions in alloys systems, including: (1) the difference in the atomic size between the solute and solvent atoms must be less than 15%, (2) the crystal structures of the solute and solvent must match, (3) there are the same valence states between the solvent and solute, and (4) the solute and solvent should have similar electronegativity. Hume-Rothery rules are generally used to predict formation of continuous solid solutions in conventional metallic alloys. However, it is not clear whether such rules can be applied directly to the multi-component HEAs, as it is hard to expect that all of the alloying elements have, for example, the same crystal structure and valence electron concentration (VEC). Efforts have been devoted to developing phase selection criteria based on Hume-Rothery rules, and a few criteria, such as the atomic-size difference (δ), electronegativity difference (ΔX) and VEC, were proposed to predict the phase formation and stability in HEAs [13–17]. The parameter δ characterizes the atomic size mismatch which produces the local elastic strain and makes the system topological unstable, while the parameter ΔX reflects the tendency of forming stable intermetallic compounds and the VEC criterion effectively predicts the structure type [13].

* Corresponding authors.
E-mail addresses: wangh@ustb.edu.cn (H. Wang), chainliu@cityu.edu.hk (C.T. Liu).

http://dx.doi.org/10.1016/j.intermet.2015.01.004
0966-9795/

It is known that the quaternary equiatomic alloy, CoCrFeNi (these elements have nearly the same atomic size and small mixing enthalpy as shown in Table 1 [18]), exhibited a single FCC solid solution phase without any obvious compositional fluctuation [19], and no long-range chemical ordering was observed as well [20]. Alloying effects on the phase formation and stability of the CoCrFeNi-based alloy were investigated and it was shown that the crystalline structure, microstructural morphology and relevant mechanical properties strongly depend on the alloying elements [21–23]. For example, alloying of Pd with a large atomic radius (i.e., 0.137 nm) into the CoCrFeNi alloy resulted in an increase of the lattice parameter and lattice distortion [24], while additions of V with a large difference in the enthalpy of mixing and atom size with the constituent components also caused significant distortion of FCC solid solution and thus promoted of the formation of σ-phase with a tetragonal crystal lattice [25]. In the $(FeCoNiCrMn)_{100-x}Al_x$ HEA system [22], the as-cast structure evolves from the initial single FCC structure to a duplex FCC plus BCC structure, and then a single BCC structure with increasing the Al concentration. In the $AlCoCrFeNiNb_x$ alloy system, it was found that additions of Nb ($x \geq 0.25$) caused the precipitate of a Laves phase with a HCP structure, and as the Nb content is increased, the resultant microstructure changed from hypoeutectic to hypereutectic and such transition had a striking effect on the compressive yielding strength and Vickers hardness [26]. However, the presence of Al makes it impossible to clearly clarify effects of Nb on the phase stability of the CoCrFeNi-based alloys since aluminum is a strong BCC stabilizer and its addition into this system are a major complication for the strengthening and phase formation [22].

In this study, we selected the CoCrFeNi alloy as the base alloy and Nb as the alloying element based on the following reasons: (1) the Nb element has been successfully used to synthesize the Ti–Al–Nb high temperature, low density intermetallic materials [27,28], (2) Nb has a large negative enthalpy of mixing with the other constituent elements (i.e., the value of Nb–Co, Nb–Cr, Nb–Fe, Nb–Ni atomic pairs is −25, −7, −16 and −30 kJ/mol, respectively [18]), and (3) Nb has the largest atomic size in this alloy system which may be favorable for the forming secondary phases, resulting in effective precipitation strengthening. Therefore, the CoCrFeNiNb_x HEAs ($x = 0$, 0.103, 0.155, 0.206, 0.309 and 0.412) were synthesized and investigated in detail.

2. Experimental

Alloy ingots with a nominal composition of $CoCrFeNiNb_x$ ($x = 0$, 0.103, 0.155, 0.206, 0.309 and 0.412, corresponding to 0, 2.52, 3.72, 4.88, 7.16 and 9.32 at %, respectively) were synthesized by arc-melting a mixture of pure metals (purity > 99.9 wt.%) in a Ti-gettered high-purity argon atmosphere. The ingots were re-melted at least five times to ensure a chemical homogeneity. Melted alloys were eventually drop-cast into a Cu mold with a dimension of 10 mm × 10 mm × 60 mm. The weight changes were recorded before and after casting, and there is no any significant mass loss. So the nominal composition should be close to the actual composition.

Table 1
Mixing enthalpy of different atom-pairs ΔH_{AB}^{mix} (kJ/mol) calculated by Miedema's approach [18].

Element (atom size, melting point)	Co	Cr	Fe	Ni	Nb
Co (0.1251 nm, 1495 °C)	–	−4	−1	0	−25
Cr (0.1249 nm, 1857 °C)	–	–	−1	−7	−7
Fe (0.1241 nm, 1535 °C)	–	–	–	−2	−16
Ni (0.1246 nm, 1453 °C)	–	–	–	–	−30
Nb (0.1429 nm, 1950 °C)	–	–	–	–	–

Phase identification of all the specimens was conducted by X-ray diffraction (XRD) using Cu Kα radiation (MXP21VAHF). Microstructure of the as-cast specimens was characterized using a Zeiss Supra55 scanning electron microscope (SEM) operated at 15 kV with an energy dispersive spectrometer (EDS). For microstructural observation, the samples were sequentially ground and then electrolyte-polished and etched with a solution composed of perchloric acid and alcohol (in a volume ratio of 1:9). While the EDS analysis was conducted on well-polished samples without etching. Volume fractions of different phases in the alloys were measured from micrographs employing a commercial software package (Image-Pro Plus). Tensile samples with a gauge length of 15 mm, a width of 4 mm and an approximate thickness of 1.2 mm were prepared from the as-cast ingots via electric discharging machining. Tensile tests were carried out on a CMT4105 universal tensile testing machine with a strain rate of 1×10^{-3} s^{-1} at room temperature. The tensile samples were sequentially ground and there is no defect was observed. Twice tests were conducted per composition.

3. Results

3.1. XRD analysis

XRD patterns from the as-cast $CoCrFeNiNb_x$ ($x = 0$, 0.103, 0.155, 0.206, 0.309 and 0.412) alloys (denoted as Nb_x hereafter) are shown in Fig. 1. The pattern of the base CoCrFeNi alloy indicates the

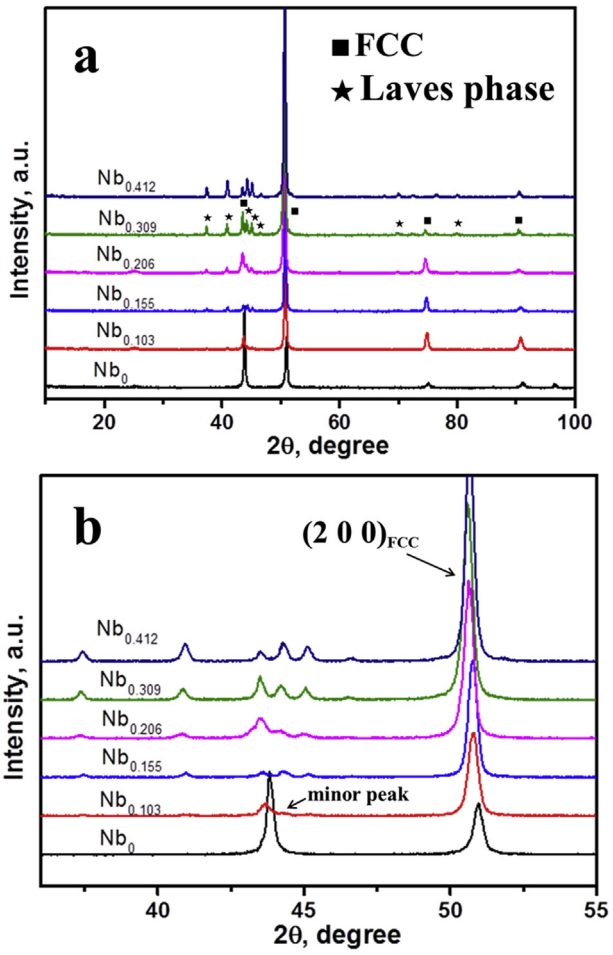

Fig. 1. (a) XRD patterns of the as-cast $CoCrFeNiNb_x$ ($x = 0$, 0.103, 0.155, 0.206, 0.309 and 0.412) alloys and (b) the detailed scans for the peak of (2 0 0) of the FCC phase.

formation of a single phase with the FCC lattice. However, with additions of 0.103 Nb (i.e., alloy $Nb_{0.103}$), a minor reflection peak around $(1\ 1\ 1)_{FCC}$ corresponding to the Laves phase appeared as shown in Fig. 1b. With increasing the Nb content, more reflection peaks corresponding to the Laves phase can be obviously observed in the $Nb_{0.155}$, $Nb_{0.206}$, $Nb_{0.309}$, and $Nb_{0.412}$ alloys. The Laves phase was identified as the $(Co,Cr,Fe,Ni)_2(Cr,Nb)$ type with a HCP lattice structure and the lattice parameters are a = 0.4801 nm and c = 0.7817 nm. Meanwhile, as shown in Fig. 1b, with the increment of the Nb content from 0.103 to 0.412, the relative intensity of the FCC diffraction peak is reduced while that of the Laves diffraction peaks is enhanced, due to the decreased volume fraction of the FCC phase relative to the Laves phase. Furthermore, the relative intensity of the Laves phase is evidently lower than that of the FCC solid solution phase, revealing that the main phase is still the latter in the alloy system. Moreover, the detailed scans for the (2 0 0) peak of the FCC solid solution phase are also shown in Fig. 1b. It is noticed that this peak shifts towards a lower 2θ angle as $x \leq 0.309$ while towards a higher 2θ angle as $x \geq 0.412$. This trend is identical to the variation of the lattice parameters of the FCC solid solution phase, which are estimated to be 0.3581, 0.3590, 0.3602, 0.3604, 0.3606 and 0.3600 nm from the strongest $(2\ 0\ 0)_{FCC}$ peak. In addition, the lattice parameter difference of the FCC solid solution as a function of the Nb content was depicted in Fig. 2. The lattice parameter difference can be expressed as $\Delta a/a_0$, where $\Delta a = |a - a_0|$, here, the lattice parameter of the CoCrFeNi alloy is considered as base in order to investigate the effect of Nb additions on the lattice parameter difference [29]. As shown, the lattice parameter difference initially increases until the Nb content reaches 0.309 and slightly drops in alloy $Nb_{0.412}$. It seems that the alloying of Nb with a large atomic radius (i.e., 0.1429 nm) into the CoCrFeNi alloy resulted in an increase of the lattice parameters.

3.2. Microstructure evolution

Microstructures of the as-cast alloys with a different Nb content were displayed in Figs. 3 and 4. Fig. 3 exhibits the low magnification morphologies and the details of different phases are shown in Fig. 4 with high magnification morphologies. The base CoCrFeNi alloy exhibiting a typical columnar crystal morphology has a single phase structure consisting of slightly elongated grains with the average width of about 150–200 μm (see Figs. 3 and 4a), which is confirmed to be the FCC phase according to the XRD pattern shown in Fig. 1. The measured composition of the grains is reasonably close to the nominal one of the alloy (Table 2). However, a small amount of white precipitates were observed in the $Nb_{0.103}$ alloy (see Figs. 3 and 4b), which corresponds to the minor peak mentioned in the XRD analysis (Fig. 1b). In alloy $Nb_{0.155}$, the columnar crystal structure gradually changes to dendrites, and the Laves phase preferred to form in the interdendritic regions (see Figs. 3 and 4c). With additions of more Nb, the morphology of the $Nb_{0.206}$, $Nb_{0.309}$ and $Nb_{0.412}$ alloys displays a typical hypoeutectic structure (see Fig. 3d–f), although the primary phase is still the FCC solid solution phase. The eutectic structure consists of a mixture of the FCC phase and the Laves phase (see Fig. 4d–f) which constitutes a continuous network. Meanwhile, with increasing the Nb content, the volume fraction of the Laves phase increases accordingly. Chemical composition of the FCC phase and the Laves phase was analyzed using the EDS and the results were listed in Table 2. The EDS analysis indicates that the FCC phase was enriched in Fe, Co with limited Nb, while Cr and Fe were depleted but Nb was enriched in the Laves phase.

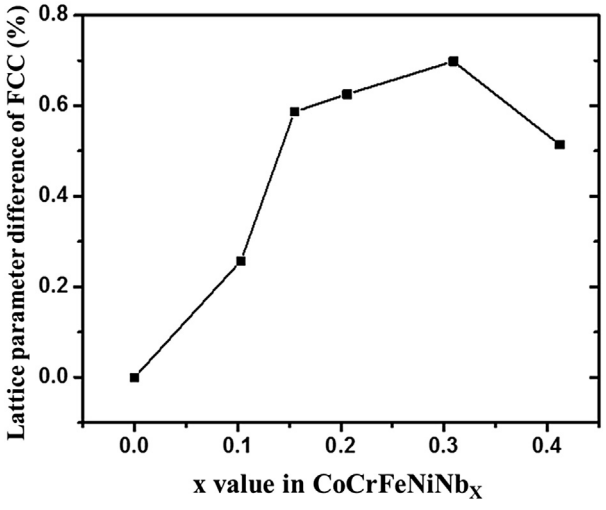

Fig. 2. Lattice parameter difference of the FCC solid solutions as a function of the Nb content in the as-cast $CoCrFeNiNb_x$ (x = 0, 0.103, 0.155, 0.206, 0.309 and 0.412) alloys.

3.3. Mechanical properties

Room-temperature tensile tests were performed to investigate effects of Nb additions on the mechanical properties of the as-cast $CoCrFeNiNb_x$ alloy system. Typical engineering stress–strain curves for the current HEAs containing different amounts of Nb are depicted in Fig. 5. The fracture strength, yield strength, and tensile ductility as a function of the Nb content are summarized in Table 3. It is noted that both the fracture and yield strengths increase as the Nb concentration increases. Specifically, the fracture and yield strengths of alloy Nb_0 are 413 and 147 MPa, respectively, but increase significantly to 1004 and 637 MPa, respectively, in alloy $Nb_{0.412}$. In contrast, the tensile elongation reduces appreciably from 49.1% in alloy Nb_0 to 1.3% in alloy $Nb_{0.412}$.

To further identify the underlying mechanism of the ductility variation in these alloys, their fracture surfaces after the tensile deformation were carefully examined by SEM, as shown in Fig. 6. Dimples with features of typical plastic fracture were observed for the Nb_0 alloy in Fig. 6a. The dimple pattern can still be found for the $Nb_{0.103}$, $Nb_{0.155}$, $Nb_{0.206}$, $Nb_{0.206}$ and $Nb_{0.412}$ alloys as demonstrated in Fig. 7b–f, however, the diameter and depth of the dimples appear to be smaller than that of the Nb_0 alloy due to the formation of the ordered Nb-enriched Laves phase.

4. Discussion

4.1. Phase selection

Based on limited experimental work on HEAs performed so far, both the enthalpy of mixing ΔH_{mix} and the atomic size difference δ were found to play dominant roles in controlling the phase selection in HEAs. Experimental results indicate that solid solutions in HEAs upon rapid solidification are favored in the regions of $-15 < \Delta H_{mix} < 5$ kJ/mol and $\delta \leq 6.6\%$, and intermetallic compounds form only in the HEAs with a quite negative $\Delta H_{mix} < -15$ kJ/mol and a large $\delta > 6.6\%$ [13,17].

For the current Nb-containing alloys, the ΔH_{mix} and δ were listed in Table 4 and the ΔH_{mix}–δ graph for the current alloy system is plotted in Fig. 7. It can be seen in Table 4 that the ΔH_{mix} value of the alloy system ranges between −5.48 and −9.68 kJ/mol and δ is between 2.3 and 4.2%. Therefore, all these alloys fall into the single solid solution zone marked with the dotted line as shown in Fig. 7. However, the Nb-enriched Laves phase even appeared in the

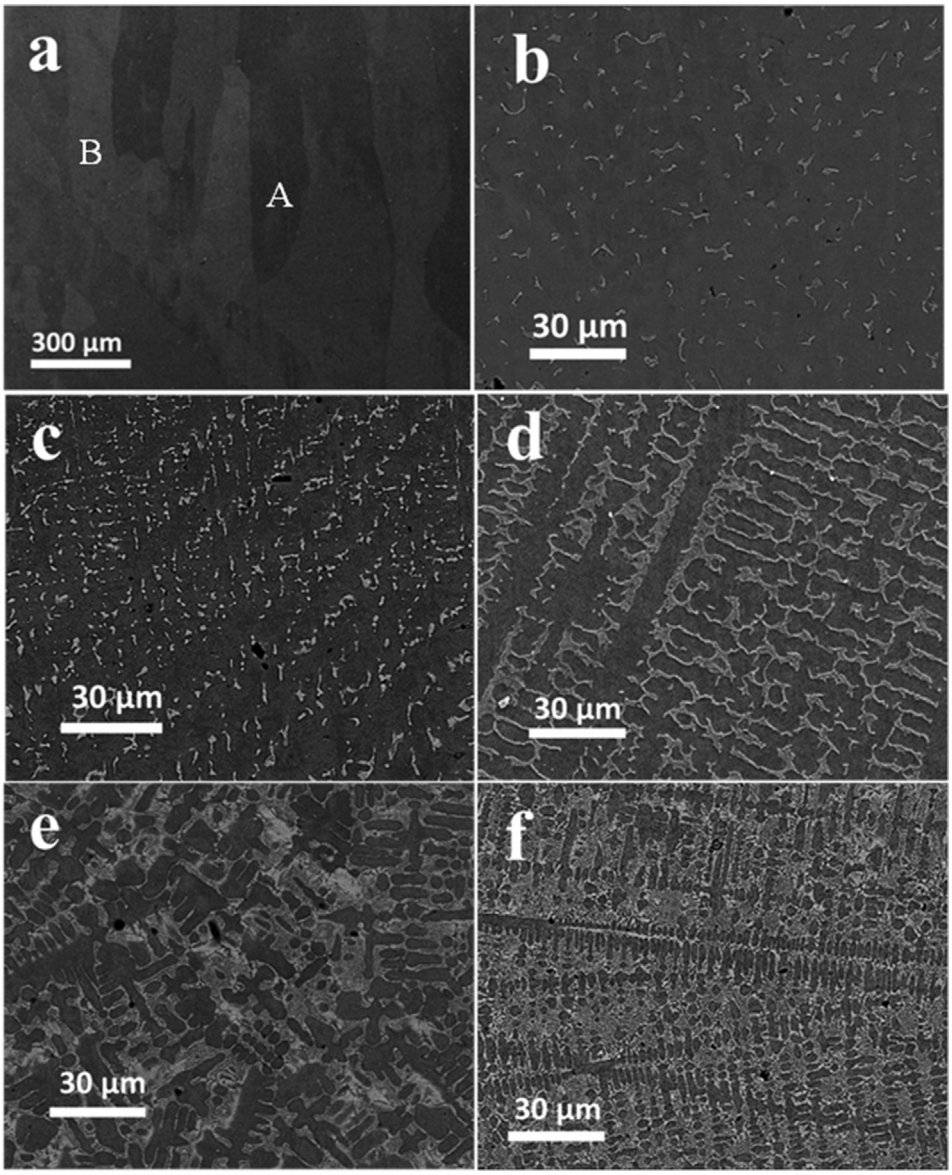

Fig. 3. SEM images of the as-cast $CoCrFeNiNb_x$ alloys. (a) x = 0, (b) x = 0.103, (c) x = 0.155, (d) x = 0.206, (e) x = 0.309 and (f) x = 0.412.

$Nb_{0.103}$ alloy, and thus the ΔH_{mix}–δ criteria fail to predict the phase selection in the current alloy system.

The phase selection criteria in HEAs discussed above was established on the as-cast samples upon rapid solidification using copper molds [13,17]. It was argued that thermal treatments of the as-cast HEAs could induce phase transformation, although the sluggish diffusion effect could generally retard the solid phase transformation [30,31]. Wang et al. modified the ΔH_{mix}–δ criteria for the equilibrium phase selection at the temperatures within $0.5 < T/T_m < 0.9$ (T_m: melting point), and they found that the boundary for forming the solid solutions shrinks to $\Delta H_{mix} \geq -7.5$ kJ/mol and $\delta < 3.3\%$ after thermal or thermo-mechanical treatments [32], which is marked with the broken line in Fig. 7. The cross section of the cast ingots is 10 × 10 mm, and it can't be totally classified as a fast cooling scope which normally requires thin cross sections less than 4 × 4 mm. So the ΔH_{mix}–δ criteria for thermal-treated alloys can used to analyze the phase selection of the Nb-containing alloy system. It can be seen in Fig. 7 that the modified criteria better depict the phase selection in the Nb-containing alloy system. Based on our experimental data, the solid solution region can be obtained in a rather narrowed region with $\Delta H_{mix} \geq -6.3$ kJ/mol and $\delta < 2.8\%$, indicating that the constituent elements for forming single solid solutions in multiple component systems should be chemically compatible.

As discussed above, the ΔH_{mix}–δ criteria cannot effectively predict formation of the topologically close-packed (TCP) phases like the Laves phase in the current alloys. Dong et al. proposed a parameter, ΔX ($= \sqrt{\sum_{i=1}^{N} C_i (X_i - \overline{X})^2}$, X_i is the Pauling electronegativity for the ith element, and $\overline{X} = \sum_{i=1}^{N} C_i X_i$ is the average eletronegativity), to predict the tendency for forming all types of TCP phases, including the Laves phase, σ phase, R phase, and μ phase [33,34]. It was confirmed that the TCP phases can form when the ΔX value reaches 0.133 and are stable at $\Delta X > 0.133$ except for some HEAs which contain a significant amount of Al [34]. The values of ΔX for the current alloy system are given in Table 4, and all of them are smaller than 0.133, however, the Nb-enriched Laves phase formed in all the Nb containing alloys. Therefore, this parameter proposed from considerations of electronegativity also fails to predict the appearance of the Nb-enriched Laves phase. The VEC for

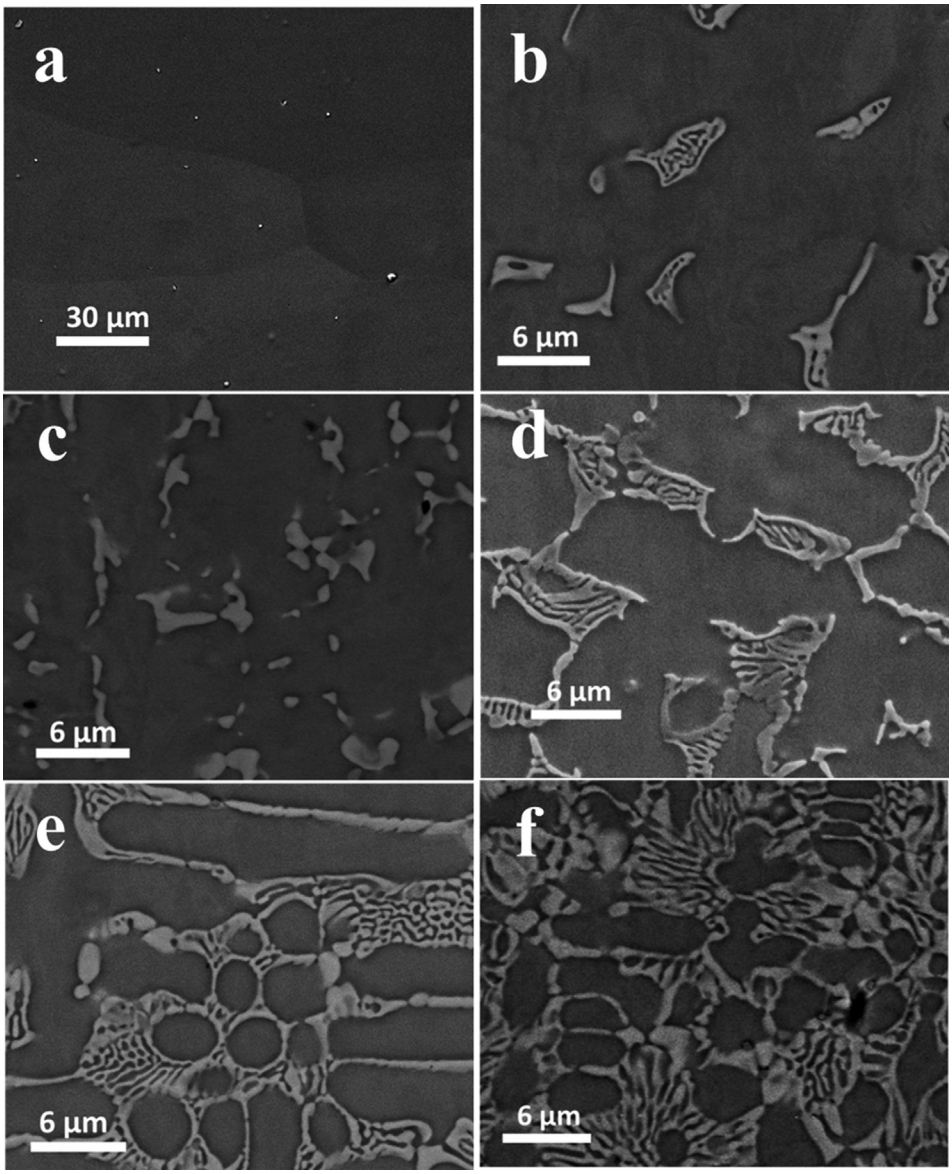

Fig. 4. High magnification SEM images of the as-cast $CoCrFeNiNb_x$ alloys. (a) x = 0, (b) x = 0.103, (c) x = 0.155, (d) x = 0.206, (e) x = 0.309 and (f) x = 0.412.

Table 2
Chemical compositions of the as-cast $CoCrFeNiNb_x$ (x = 0, 0.103, 0.155, 0.206, 0.309 and 0.412) alloys.

Alloys	Region	Cr	Fe	Co	Ni	Nb
Nb_0	Nominal	25.00	25.00	25.00	25.00	0.00
	A	20.23	30.21	25.23	24.32	0.00
	B	20.83	26.12	25.43	27.63	0.00
$Nb_{0.103}$	Nominal	24.37	24.37	24.37	24.37	2.52
	Base	21.30	28.46	24.68	23.84	1.73
	Precipitate	14.57	18.39	23.14	22.74	21.17
$Nb_{0.155}$	Nominal	24.07	24.07	24.07	24.07	3.72
	Base	21.11	27.49	25.11	24.47	1.82
	Precipitate	12.51	16.90	23.25	19.43	27.91
$Nb_{0.206}$	Nominal	23.78	23.78	23.78	23.78	4.88
	Base	20.46	26.39	25.10	24.94	3.10
	Precipitate	16.44	21.42	23.94	22.76	15.43
$Nb_{0.309}$	Nominal	23.21	23.21	23.21	23.21	7.16
	Base	21.68	27.68	23.34	24.15	3.16
	Precipitate	13.65	17.26	24.19	20.41	24.50
$Nb_{0.412}$	Nominal	22.67	22.67	22.67	22.67	9.32
	Base	22.05	28.43	23.07	22.60	3.85
	Precipitate	13.92	19.70	22.18	17.45	26.75

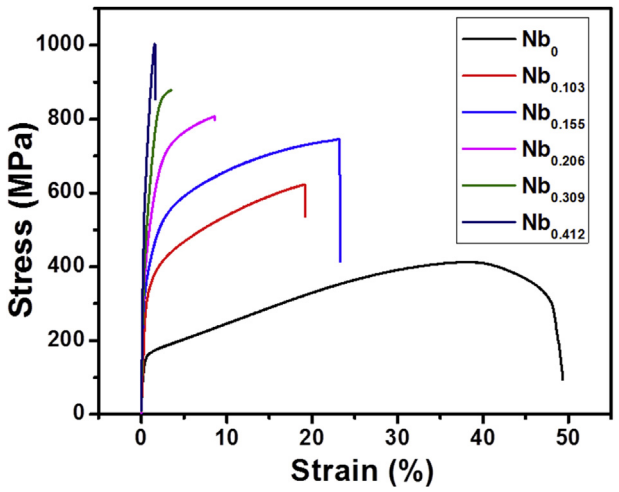

Fig. 5. Engineering tensile stress–strain curves of the as-cast $CoCrFeNiNb_x$ (x = 0, 0.103, 0.155, 0.206, 0.309 and 0.412) alloys at room temperature.

Table 3
Tensile properties of the as-cast $CoCrFeNiNb_x$ (x = 0, 0.103, 0.155, 0.206, 0.309 and 0.412) alloys.

Alloys	$\sigma_{0.2}$ (MPa)	σ_{max} (MPa)	ε(%)
Nb_0	147	413	48.0
$Nb_{0.103}$	317	622	19.2
$Nb_{0.155}$	321	744	23.3
$Nb_{0.206}$	402	807	8.6
$Nb_{0.309}$	478	879	3.5
$Nb_{0.412}$	637	1004	1.3

this Nb-containing alloy system were listed in Table 4, and it ranges between 8.25 and 7.95. It's obvious all the other alloys are in the FCC zone except the alloy $Nb_{0.412}$ falling into the FCC + BCC zone. This criterion also failed to forecast the appearance of the Laves phase. As discussed above, all the criteria, i.e., ΔH_{mix}—δ, VEC and ΔX, cannot effectively predict the phase formation in the current Nb-containing HEA system and describe the alloying effect of Nb.

In our previous work [12], we argued that the large mixing entropy and small enthalpy of mixing may not be sufficient to prevent the segregation of the elements chemically incompatible with each other, and the effects of the mixing enthalpy between the constituent atomic pairs ΔH_{AB}^{mix}, and the non-configurational entropy on phase formation should also be considered, particularly in the cases with additions of chemically incompatible elements. The intermetallic compounds can form even the alloys were rapidly quenched if the mixing enthalpy ΔH_{AB}^{mix} between certain atomic pairs is large enough, although the total mixing enthalpy ΔH_{mix} is still small. It is particularly pointed out that the Nb atom has a larger radius than the other transition metals in the alloy system. Thus, the solutioning of the Nb element into CoCrFeNi is expected to distort the lattice. From Fig. 2, it is known that the lattice parameter difference is initially increased with the increase of the Nb content, which causes an apparent lattice straining effect. In other words, the large lattice distortion energy is produced, which destabilizes the FCC matrix and promotes the formation of the Nb-enriched Laves phase. Furthermore, Nb has large negative enthalpies of mixing with the other alloying elements. As shown in Table 1, the mixing enthalpy ΔH_{AB}^{mix} of the Nb element with any of the Fe, Cr, Ni, Co elements is far below zero. Mixing enthalpy ΔH_{AB}^{mix} reflects the driving force for forming stable intermetallic compounds; consequently, addition of the Nb element is inclined to form intermetallics phases with the Fe, Cr,

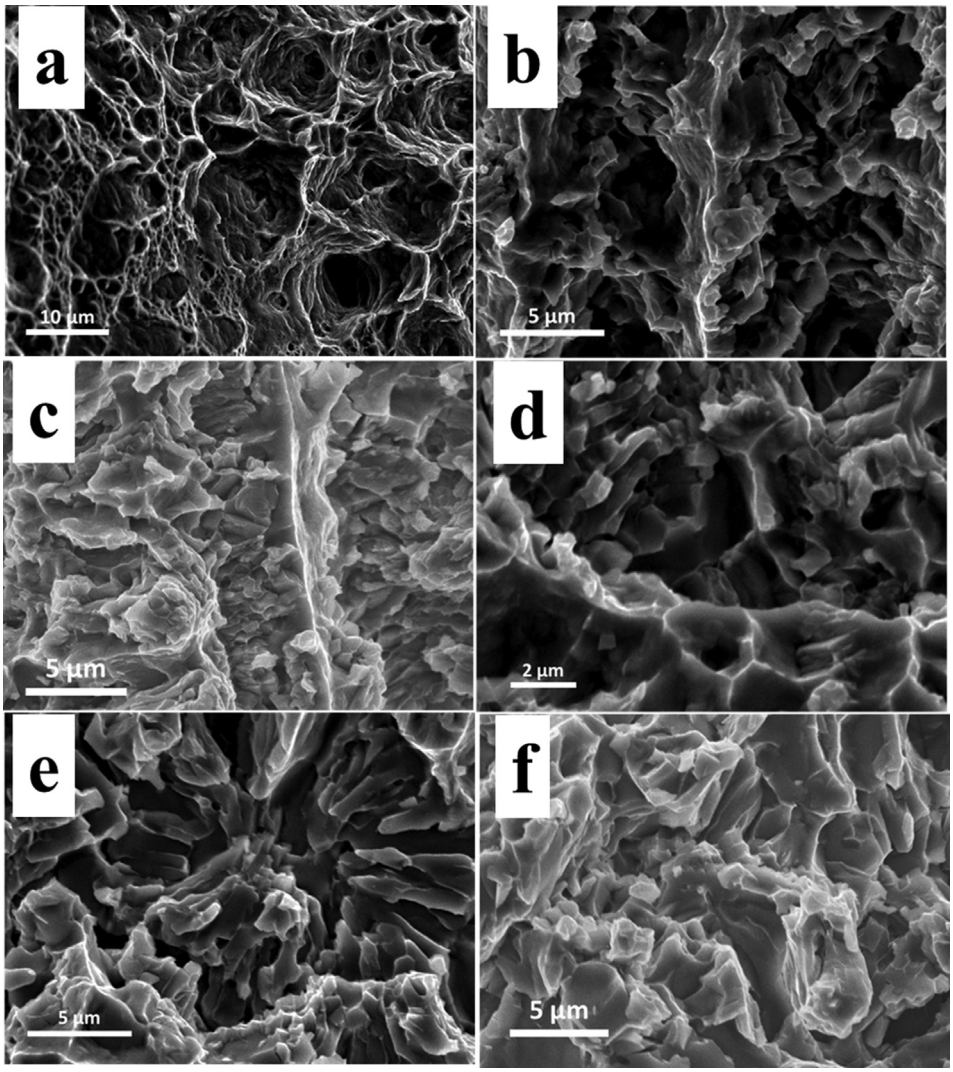

Fig. 6. SEM secondary electron images of the fractured surfaces after the tensile deformation for the as-cast $CoCrFeNiNb_x$ alloys. (a) x = 0, (b) x = 0.103, (c) x = 0.155, (d) x = 0.206, (e) x = 0.309 and (f) x = 0.412.

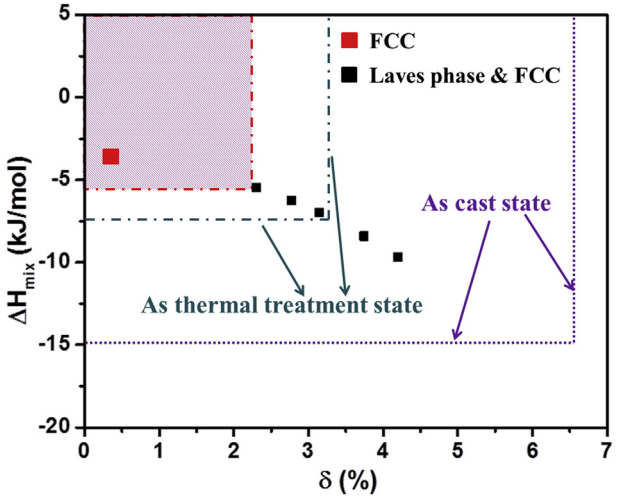

Fig. 7. The ΔH_{mix}-δ criterion for the as-cast $CoCrFeNiNb_x$ ($x = 0$, 0.103, 0.155, 0.206, 0.309 and 0.412) alloys. The dotted line delineates the solid solution region for the as-cast alloys [13,17], the broken line depicts the solid solution region for the alloys thermally treated [32], and the narrowed as-cast solid solution region indicated by the shaded area after including the current alloy system.

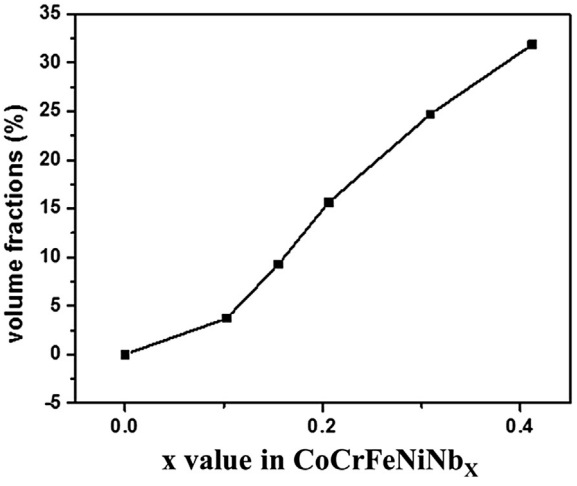

Fig. 8. The volume fractions of the Nb-enriched Laves phase as a function of the Nb content for the as-cast $CoCrFeNiNb_x$ ($x = 0$, 0.103, 0.155, 0.206, 0.309 and 0.412) alloys.

Ni, Co elements, especially for the NiNb pair because of its lowest mixing enthalpy ΔH_{AB}^{mix}. As a result, the Nb-enriched Laves phase is prone to form even if the total Nb content is low due to the large mixing enthalpies ΔH_{AB}^{mix} of the Nb element with the other constituents in the alloys.

4.2. Relationship between the microstructure and tensile properties

It is apparent that in the present alloy system, the $Nb_{0.155}$ alloy has the most promising tensile properties; its yield strength, fracture strength, and plastic strain are as high as 321 MPa, 744 MPa and 21.3%, respectively. The excellent tensile properties of the $Nb_{0.155}$ alloy are attributed to a combination of the solid-solution strengthening from the Nb atoms and the second-phase hardening from the ordered Nb-enriched Laves phase in the FCC matrix. In the $Nb_{0.155}$ alloy, solid-solutioned Nb atoms greatly enhance the lattice distortion in the FCC matrix due to their large atomic size, as presented in Fig. 2. Furthermore, formation of the ordered Nb-enriched Laves phase significantly enhances the strength of the HEAs due to the precipitation hardening effect, while the main phase of the $Nb_{0.155}$ alloy, i.e., the FCC matrix, provides good plastic properties. Such the composite structure in the $Nb_{0.155}$ alloy gave rise to excellent overall tensile properties. It appears that the sharp drop of the ductility in the alloys containing a high Nb amount (e.g., alloy $Nb_{0.206}$) is due to the formation of the interconnected brittle Laves-phase patches, as shown in Fig. 4c–d. Cracks were formed in the ordered Nb-enriched Laves-phase patches, which deteriorates the alloys plasticity. With increasing of the Nb content, the volume fraction of the ordered Nb-enriched Laves phase increases, further embrittling the alloys.

Moreover, the volume fraction of the Nb-enriched Laves phase in this alloy system can be defined as f_L = Laves/(FCC + Laves), and its changes as a function of the Nb content is plotted in Fig. 8 and the corresponding data of f_L are given in Table 4. It can be seen that f_L increases from 0% to 31.9% with increasing of the Nb content. Thus, the massive distribution of the Nb-enriched Laves phase along the interdendrites impeded the dislocation movement, which has an important impact on the yield strength. However, the plasticity of these alloys was obviously deteriorated as a result of the increase of the amount of the brittle Nb-enriched Laves phase.

Table 4
Calculated parameters ΔH_{mix}, δ, ΔX, VEC and f_L for the studied alloys.

Alloys	ΔH_{mix} (kJ/mol)	δ (%)	ΔX	VEC	Phase(s)	f_L (%)
Nb_0	−3.7	0.3%	0.097	8.25	FCC	0
$Nb_{0.103}$	−5.5	2.3%	0.101	8.17	FCC + Laves	3.7%
$Nb_{0.155}$	−6.3	2.8%	0.104	8.13	FCC + Laves	9.3%
$Nb_{0.206}$	−7.0	3.1%	0.105	8.09	FCC + Laves	15.6%
$Nb_{0.309}$	−8.4	3.7%	0.110	8.02	FCC + Laves	24.7%
$Nb_{0.412}$	−9.7	4.2%	0.112	7.95	FCC + Laves	31.9%

5. Conclusion

In conclusion, additions of the Nb element into the CoCrFeNi HEA changed the original phase constitution and led to the formation of an ordered Nb-enriched Laves phase embedded in the FCC solid solution matrix. Furthermore, the criteria of ΔH_{mix}–δ cannot reflect the precipitation of the Nb-enriched Laves phase in the current alloy system. Another criterion, ΔX, proposed to predict the appearance of TCP phases in HEAs also failed to represent the phase changes with the Nb additions. In addition to the mixing enthalpy, the atomic size difference and the electronegativity difference, the mixing enthalpy of certain atom pairs, namely ΔH_{AB}^{mix} should be also considered as far as the phase selection and stability of HEAs are concerned. The base alloy without Nb exhibits an excellent ductility with an elongation of 48.0%, but the yield and fracture strengths are relatively low. After the precipitation of the Nb-enriched Laves phase, the strength is drastically increased. Among these alloys, the $Nb_{0.155}$ alloy containing a volume fraction of 9.3% Laves phase exhibited the most promising tensile properties with the yield strength, fracture strength and plastic strain as high as 321 MPa, 744 MPa and 21.3%, respectively. This particular alloy with strong solid-solution strengthening and precipitation hardening resulted from the Nb additions can be a good candidate for engineering applications at varied temperatures.

Acknowledgments

This research was supported by GRF project number CityU 521411. HW and ZPL acknowledge financial support from National Natural Science Foundation of China (Nos.51010001, 51001009, and 51271212), and 111Project (B07003).

References

[1] Yeh JW, Chen SK, Lin SJ, Gan JT, Chin TS, Shun TT, et al. Adv Eng Mater 2004;6:299–303.
[2] Singh S, Wanderka N, Murty BS, Glatzel U, Banhart J. Acta Mater 2011;59:182–90.
[3] Huang YS, Chen L, Lui HW, Cai MH, Yeh JW. Mater Sci Eng A 2007;457:77–83.
[4] He JY, Zhu C, Zhou DQ, Liu WH, Nieh TG, Lu ZP. Intermetallics 2014;55:9–14.
[5] Chuang MH, Tsai MH, Wang WR, Lin SJ, Yeh JW. Acta Mater 2011;59:6308–17.
[6] Zhou YJ, Zhang Y, Wang YL, Chen GL. Mater Sci Eng A 2007;454–455:260–5.
[7] Liu WH, Wu Y, He JY, Nieh TG, Lu ZP. Scr Mater 2013;68:526–9.
[8] Widom M, Huhn WP, Maiti S, Steurer W. Metall Mater Trans A 2014;45:196–200.
[9] Tong CJ, Chen YL, Chen SK, Yeh JW, Shun TT, Tsau CH, et al. Metall Mater Trans A 2005;36:881–93.
[10] Zhu JM, Fu HM, Zhang HF, Wang AM, Li H, Hu ZQ. Mater Sci Eng A 2010;527:7210–4.
[11] Otto F, Yang Y, Bei H, George EP. Acta Mater 2013;7:2628–38.
[12] Liu WH, Wu Y, He JY, Zhang Y, Liu CT, Lu ZP. JOM 2014;66:1973–83.
[13] Zhang Y, Zhou YJ, Lin JP, Chen GL, Liaw PK. Adv Eng Mater 2008;10:534–8.
[14] Guo S, Liu CT. Prog Nat Sci 2011;21:433–46.
[15] Guo S, Ng C, Lu J, Liu CT. J Appl Phys 2011;109:103505–15.
[16] Yang X, Zhang Y. Mater Chem Phys 2012;132:233–8.
[17] Guo S, Hu Q, Ng C, Liu CT. Intermetallics 2013;41:96–103.
[18] Takeuchi A, Inoue A. Mater Trans 2005;46:2817–29.
[19] Gali A, George EP. Intermetallics 2013;39:74–8.
[20] Lucas MS, Wilks GB, Mauger L, Munoz JA, Senkov ON, Michel E, et al. Appl Phys Lett 2012;100:2519507–14.
[21] Wu JM, Lin SJ, Yeh JW, Chen SK, Huang YS, Cheng HC. Wear 2006;261:513–9.
[22] He JY, Liu WH, Wang H, Wu Y, Liu XJ, Nieh TG, et al. Acta Mater 2013;62:105–13.
[23] Wang XF, Zhang Y, Qiao Y, Chen GL. Intermetallics 2007;15:357–62.
[24] Lucas MS, Mauger L, Muñoz JA, Xiao YM, Sheets AO, Semiatin SL, et al. Appl Phys 2011;109:07E307–13.
[25] Salishchev GA, Tikhonovsky MA, Shaysultanov DG, Stepanov ND, Kuznetsov AV, Kolodiy IV, et al. J Alloy Compd 2014;591:11–21.
[26] Ma SG, Zhang Y. Mater Sci Eng A 2012;532:480–6.
[27] Chen GL, Wang XT, Ni KQ, Hao SM, Cao JX, Ding JJ, et al. Intermetallics 1996;4:13–22.
[28] Qiao JW, Zhang Y. Intermetallics 2011;19:149–53.
[29] Zhu JM, Fu HM, Zhang HF, Wang AM, Li H, Hu ZQ. Mater Sci Eng A 2010;527:6975–9.
[30] Ng C, Guo S, Luan J, Shi S, Liu CT. Intermetallics 2012;31:165–72.
[31] Tsai KY, Tsai MH, Yeh JW. Acta Mater 2013;61:4887–97.
[32] Wang ZJ, Guo S, Liu CT. JOM 2014;66:1966–72.
[33] Dong Y, Lu YP, Jiang L, Wang TM, Li TJ. Intermetallics 2014;52:105–9.
[34] Fang SS, Xiao XS, Xia L, Li WH, Dong YD. J Non Cryst Solids 2003;321:120–5.